Ionics (2020) 26:2139–2145
https://doi.org/10.1007/s11581-019-03401-x

ORIGINAL PAPER

Preparation of $LiFePO_4/H_2Ti_3O_7$ and $LiFePO_4/TiO_2$ nanocomposite by sol-gel method as cathode material for lithium-ion battery

Pengqing Hou[1] · Sinan Li[1,2,3] · Liu Yang[1,2,3] · Yafeng Wang[1,2,3] · Luoxuan Wang[1,3] · Shao-hua Luo[1,3,4]

Received: 19 November 2019 / Revised: 5 December 2019 / Accepted: 10 December 2019 / Published online: 24 December 2019

Abstract

The sol-gel method is adopted for synthesizing $LiFePO_4/H_2Ti_3O_7$ and $LiFePO_4/TiO_2$ nanocomposites and contrasted them with different content. The crystal structure and morphology of the as-synthesized samples are characterized via X-ray diffraction and scanning electron microscope techniques, respectively. It is demonstrated that the structure of composite materials is a single olivine structure without any impurity phases. The specific surface area and pore size of $H_2Ti_3O_7$ and TiO_2 are analyzed using the BET surface area technique and the BJH method, which exhibits that the higher specific surface area is very beneficial to the diffusion of lithium ion. Also, the electrochemical properties are tested by the charge-discharge tests. Two composites show fascinating cycle capacity and charge-discharge performance when the amount of $H_2Ti_3O_7$ and TiO_2 is 1%. Among them, 1% $H_2Ti_3O_7$ presents a better performance at 0.5 C. The sample delivers a discharge capacity of 161.1 mAh g^{-1} (105.83% of the initial capacity is kept after 50 cycles). In conclusion, the proper addition of $H_2Ti_3O_7$ and TiO_2 can effectively facilitate the lithium ion diffusion rate to enhance the electrochemical properties of composites.

Keywords $LiFePO_4$ · $H_2Ti_3O_7$ · TiO_2 · Sol-gel method · Electrochemical performance

Introduction

In recent years, renewable and green energy such as solar, wind, and tidal power has greatly attracted the interest of scientific researchers, while the rechargeable lithium-ion batteries (LIBs) are one of the most widely used energy storage devices used in portable electronic devices and electric vehicles [1–6]. Among them, $LiFePO_4$ cathode material is considered prospective materials and attracted great interest because it is low cost, environmentally friendly, and energy dense [7–10]. However, the low electronic conductivity, as well as the slow lithium-ion diffusion rate, is the two major drawbacks of $LiFePO_4$, which restricts its performance at a high rate [11–13]. Consequently, various strategies have been attempted to overcome these problems and improve the electrochemical properties of $LiFePO_4$. Among all methods, choosing the proper composite materials and introducing into $LiFePO_4$ can effectively enhance the ionic conductivity and electronic conductivity of the active materials in the electrodes [14–16]. Medvedeva et al. synthesized $LiFePO_4$, $LiMn_2O_4$, and $LiNi_{0.82}Co_{0.18}O_2$ by ultrasonic treatment and analyzed the electrochemical performance of composites [17]. Liu et al. present a mesostructured $LiFePO_4$/reduced graphene oxide composite material which exhibits a high capacity with 161 mAh g^{-1} after 200 cycles at 0.2 C, accompanying with a Coulombic efficiency of about 100% [18]. Junhui Jeong et al. enhanced the cycling performance of LIBs by rational designing oxide/carbon composites, the rate capacity was improved which is mainly due to the enhancement of lithium-ion transport through the nanoperforations [19]. Yang et al. prepared a 3D spray-dried micro/mesoporous $LiFePO_4$/porous graphene oxide/C composite material by a three-step process: hydrothermal process, carbon coating step, and spray dry process. The SP-LFP/PGO/C composite exhibits the performance of the discharge capacity is 160, 152, 151 mAh g^{-1} at 0.1 C, 0.2 C, and 0.5 C rate [20–22].

✉ Shao-hua Luo
tianyanglsh@163.com

[1] School of Resources and Materials, Northeastern University at Qinhuangdao, Qinhuangdao 066004, People's Republic of China

[2] School of Materials Science and Engineering, Northeastern University, Shenyang 110819, People's Republic of China

[3] Key Laboratory of Dielectric and Electrolyte Functional Material Hebei Province, Qinhuangdao, People's Republic of China

[4] Qinhuangdao Laboratory of Resources Cleaner Conversion and Efficient Utilization, Qinhuangdao, People's Republic of China

In this paper, we have successfully synthesized composites with high ionic conductivity through the addition of $H_2Ti_3O_7$ and TiO_2 into $LiFePO_4$ and methodically studied the effect of composite materials on the cycling capability and rate capability. Furthermore, their crystal structure and morphology of the as-prepared composite materials have been evaluated by the X-ray diffraction and the scanning electron microscope.

Experimental

Preparation of $H_2Ti_3O_7$ and TiO_2

$H_2Ti_3O_7$ and TiO_2 were fabricated by the ultrasonic chemical hydrothermal approach. First, the TiO_2 and NaOH with a certain concentration reacted 2 h in the ultrasonic generator. Subsequently, the mixture was placed in a Teflon autoclave and hydrothermal reaction for 48 h at 120~180 °C. After the reaction, the reaction kettle and the filter cake were washed by deionized water and anhydrous alcohol several times until the pH value reached 7. Finally, the $H_2Ti_3O_7$ was obtained by drying at 80 °C under vacuum. At the same time, a part of the $H_2Ti_3O_7$ was calcinated to obtain TiO_2 in the electric stove.

Synthesis of $LiFePO_4/H_2Ti_3O_7$ and $LiFePO_4/TiO_2$ composites

In the experiment, the procedures for different contents of $LiFePO_4/H_2Ti_3O_7$ and $LiFePO_4/TiO_2$ composite materials were synthesized via the convenient sol-gel method, and high purity N_2 was used as protecting gas. Firstly, adding $LiNO_3$ and $FeCl_2{\cdot}4H_2O$ (in a 1 : 1 M ratio) to a solution of ethanol. Then, the above solution and a certain amount of nanomaterials were sequentially dissolved in $NH_4H_2PO_4$ and citric acid. After ultrasonic processing for 2 h and vacuum treatments for 12 h, the dried gel was then obtained by heat treating and magnetic stirring at 80 °C. Next, the dry gel was ground into powder and pretreatment of 6~10 h under the protection of N_2 at 450 °C. The powder was ball-milled for 4 h, dried in air, and then calcined under N_2 atmosphere at 750 °C for 6~10 h to gain composite materials of $LiFePO_4/H_2Ti_3O_7$ and $LiFePO_4/TiO_2$. The preparation process of the $LiFePO_4/H_2Ti_3O_7$ and $LiFePO_4/TiO_2$ composites is shown in Fig. 1.

Characterization

The crystal structures of the as-synthesized materials were characterized via X-ray diffraction (DX-2500) equipped with Cu Kα radiation ($\lambda = 0.15418$ nm) from $2\theta = 10$~80°, which

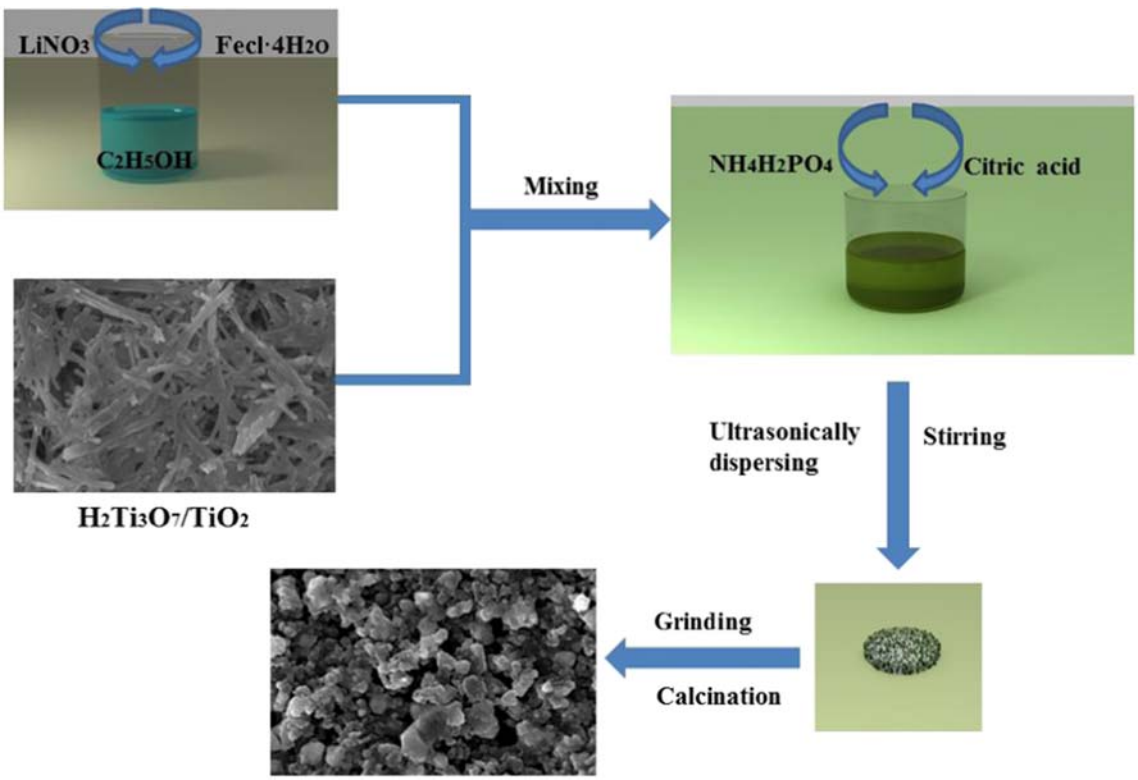

Fig. 1 Schematic illustration for the synthesis process of the composites

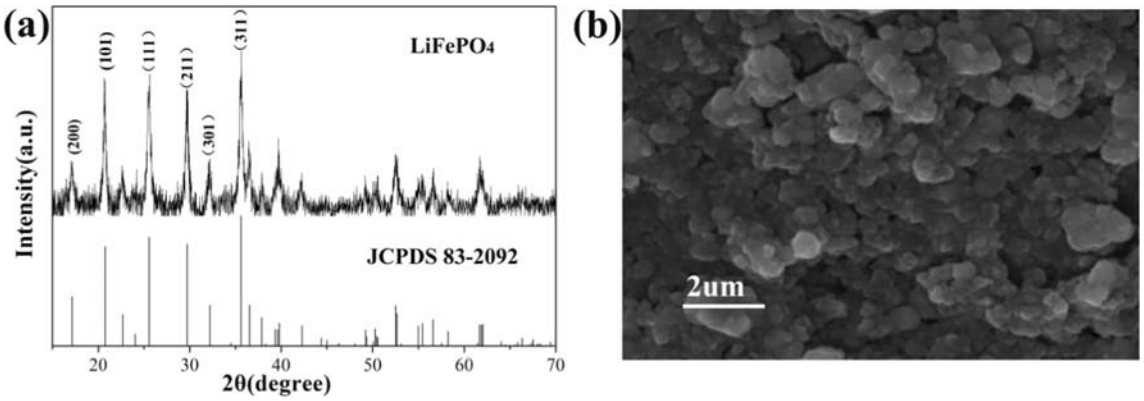

Fig. 2 **a** XRD patterns of the $LiFePO_4$. **b** SEM image of the $LiFePO_4$

the working voltage of 30 kV and the tube current of 25 mA. The surface morphologies were identified by scanning electron microscopy (SEM, SSX-550). The Brunauer-Emmett-Teller (BET) multiple points method with a specific surface area analyzer (SSA-4300) were used to measure the pore-size distribution and specific surface area. The electrochemical properties were conducted through the button cell (CR-2032) and all cells were assembled in a glove-box under the argon atmosphere. The working electrode was mixed by the 80% active materials, 10% acetylene black, and 10% polyvinylidene fluoride (PVDF). N-methyl-2-pyrrolidone (NMP) was used as a dispersant to mix them together and form a viscous slurry, followed by coating the slurry on Al foils and dried at 80 °C for 6 h to volatilize the NMP [23]. To remove excess moisture from the electrode, the working electrode should be vacuum dried in an oven at 120 °C for 8 h before assembling the battery [24]. The cathode and the separators were lithium tablets and Celgard 2400, respectively. One molar $LiPF_6$ solution was dissolved in ethylene carbonate (EC) and diethyl carbonate (DEC) at a volume ratio of 1 : 1, which was used as the electrolyte. The charge and discharge test was conducted by the Land CT2001A battery system between 2.5 and 4.2 V under room temperature.

Results and discussion

Figure 2a exhibits the XRD patterns of the $LiFePO_4$. The sample has characteristic diffraction peaks (200), (101), (111), (211), and (311), which corresponds to the olivine structure $LiFePO_4$ standard card JCPDS 83-2092. In addition, no obvious impurity phases are observed, which indicates a pure phase $LiFePO_4$ has achieved. Furthermore, the diffraction peak of the calcined $LiFePO_4$ is sharp, and the crystallinity is excellent. SEM image of as-prepared $LiFePO_4$ is shown in Fig. 1b. It is obviously seen that slight agglomeration, which is caused by the carbon. And the result is in good agreement with the XRD results [25].

The surface area and the pore-size distribution of $LiFePO_4$, $H_2Ti_3O_7$, and TiO_2 are presented in Fig. 3 and its inset, respectively. The $H_2Ti_3O_7$ and TiO_2 samples exhibit type III isotherm curves at the relative pressure of 0.2–1.0, suggesting the existence of the

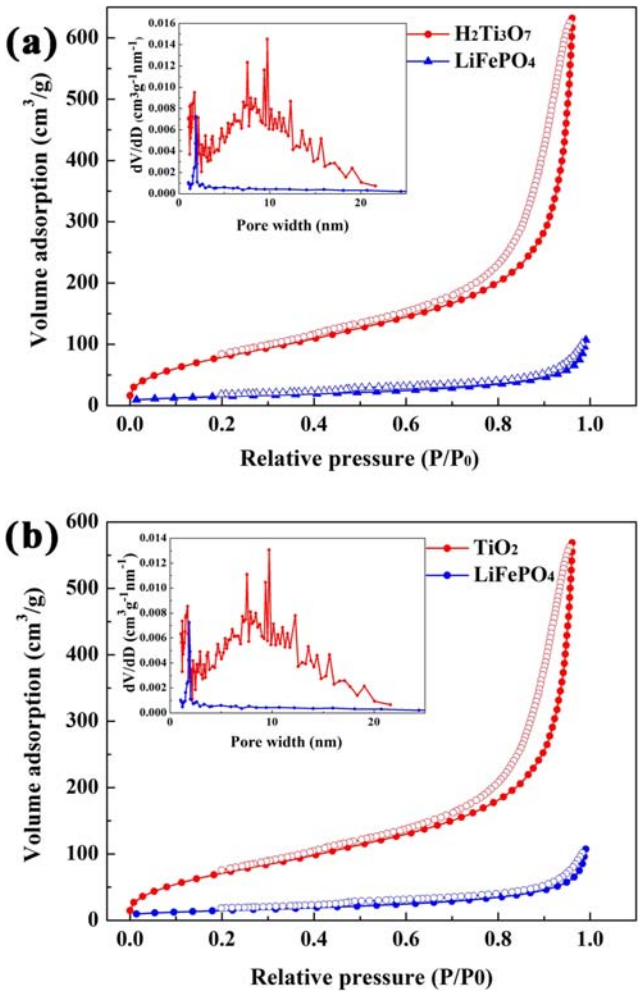

Fig. 3 N_2 adsorption and desorption isotherms of (**a**) $H_2Ti_3O_7$ and $LiFePO_4$ and (**b**) TiO_2 and $LiFePO_4$; the insert was pore-size distribution curve by the Barrette-Joyner-Halenda formula

mesoporous structure. And with increasing pressure, the adsorption increases slowly. Figure 2a exhibits that the BET specific surface area of $H_2Ti_3O_7$ (316.009 m^2/g) is much higher than that of $LiFePO_4$ (53.758 m^2/g). Moreover, the pore-size distribution of $H_2Ti_3O_7$ has distributed around 0.23 and 25.49 nm with an average pore diameter of 6.82 nm. The large specific surface area will be favorable for the electrolyte to pass through and provide more active sites for Li-ion insertion and extraction, thus accelerating the ionic and electronic diffusion [26, 27]. Figure 3b presents that the specific surface area of TiO_2 is 284.4 m^2/g. And the pore-size distribution curve displays that the pore-size is distributed between 0.6 and 23.48 nm.

Figure 4 a and b display the XRD patterns of composites with different adding amounts of $H_2Ti_3O_7$ and TiO_2. The major diffraction peaks of (200), (101), (111), (211), and (311) exist in the six composites, and the diffraction peaks position and intensities also correspond well to orthorhombic crystal system $LiFePO_4$ with olivine structure. The diffraction peaks of $H_2Ti_3O_7$ and TiO_2 are not observed in the above XRD diffraction pattern, mainly because the addition of $H_2Ti_3O_7$ nanotubes and TiO_2 nanotubes is small and the crystallinity is poor, and the diffraction peaks of A and B are "obscured" by the strong diffraction peaks of lithium iron phosphate. Furthermore, no impurity peaks are detected in the samples, which means the addition of $H_2Ti_3O_7$ and TiO_2 does not significantly change the crystal structure of $LiFePO_4$.

The SEM images of the comprised materials with 1%, 3%, and 5% $H_2Ti_3O_7$ are demonstrated in Fig. 5a–c. It is observed that the particle size distribution is varied with $H_2Ti_3O_7$ adding content. In addition, with the increase of adding amounts, particle agglomeration is decreased. For comparison, the SEM photographs of different addition of TiO_2 are displayed in Fig. 5d–f. It is found that the size of particles decreases and the size distribution is relatively uniform with TiO_2 addition contents increasing. Although both of them showed no significant difference in the morphology, the porous structure of $LiFePO_4/H_2Ti_3O_7$ composite, which can shorten the lithium-ion diffusion distance, thus provide better performance.

Figure 6 a shows the rate capacities of composites degrees with different adding amounts of $H_2Ti_3O_7$ from 0.2 to 2.0 C. Obviously, as the current density increases, all the samples present a decrease in discharge capacities systematically. Compared with the $LiFePO_4$ electrode, the $LiFePO_4/H_2Ti_3O_7$ samples exhibit a better rate of the property. In all the samples, the 1% content $LiFePO_4/H_2Ti_3O_7$ composite electrode exhibits the highest discharge capacity at 0.5 C. In addition, the 1% content $LiFePO_4/H_2Ti_3O_7$ composite electrode shows relatively moderate capacity fading, which is compared with the other samples. The maximum discharge capacity of 1% content $LiFePO_4/H_2Ti_3O_7$ at 0.5 C is 161.1 mAh g^{-1}, while that of $LiFePO_4$ is only 75.1 mAh g^{-1}.

For comparison, Fig. 6b exhibits the discharge capacities of composites degrees with different adding amounts of TiO_2 at different rate capability. It is clearly seen that the 1% TiO_2 sample exhibits more excellent rate capabilities than $LiFePO_4$. For samples at 0.2, 0.5, 1.0, and 2.0 C, the discharge capacities are 137.7, 134.9, 123.5, and 118.9 mAh g^{-1}, respectively. Obviously, the 1% content $LiFePO_4/H_2Ti_3O_7$ composite material exhibits the best rate capability among all the synthesized samples.

The initial discharge curves of 1% $H_2Ti_3O_7$ and TiO_2 from 0.2 to 2.0 C are illustrated in Fig. 6c. As observed from the curves, the $LiFePO_4/H_2Ti_3O_7$ electrode shows a superior discharge capacity to the $LiFePO_4/TiO_2$ electrode at all discharge rates. Moreover, the first discharge

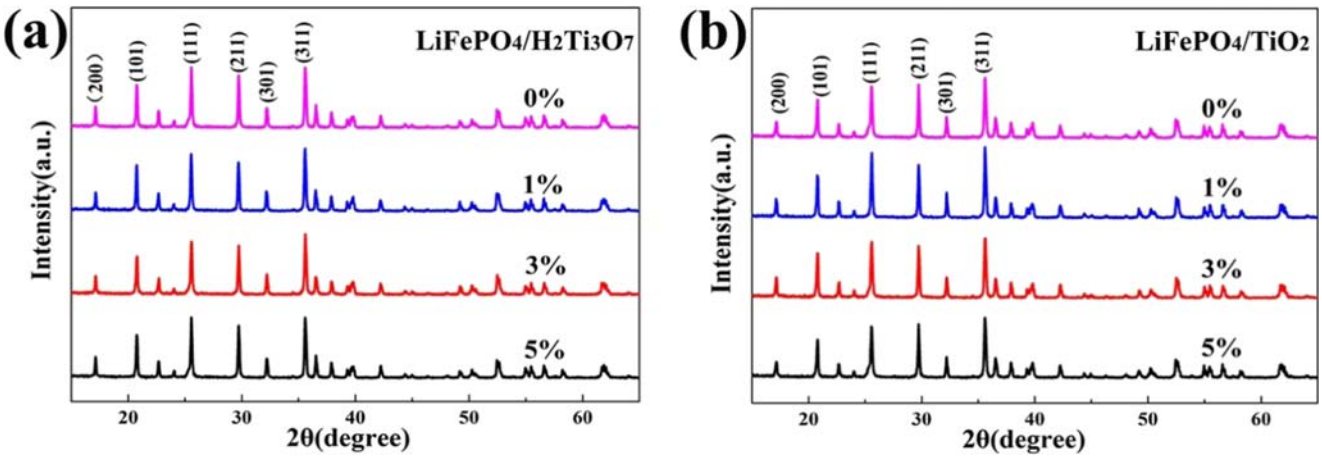

Fig. 4 XRD diffraction patterns of different adding amount: (**a**) $H_2Ti_3O_7$, (**b**) TiO_2

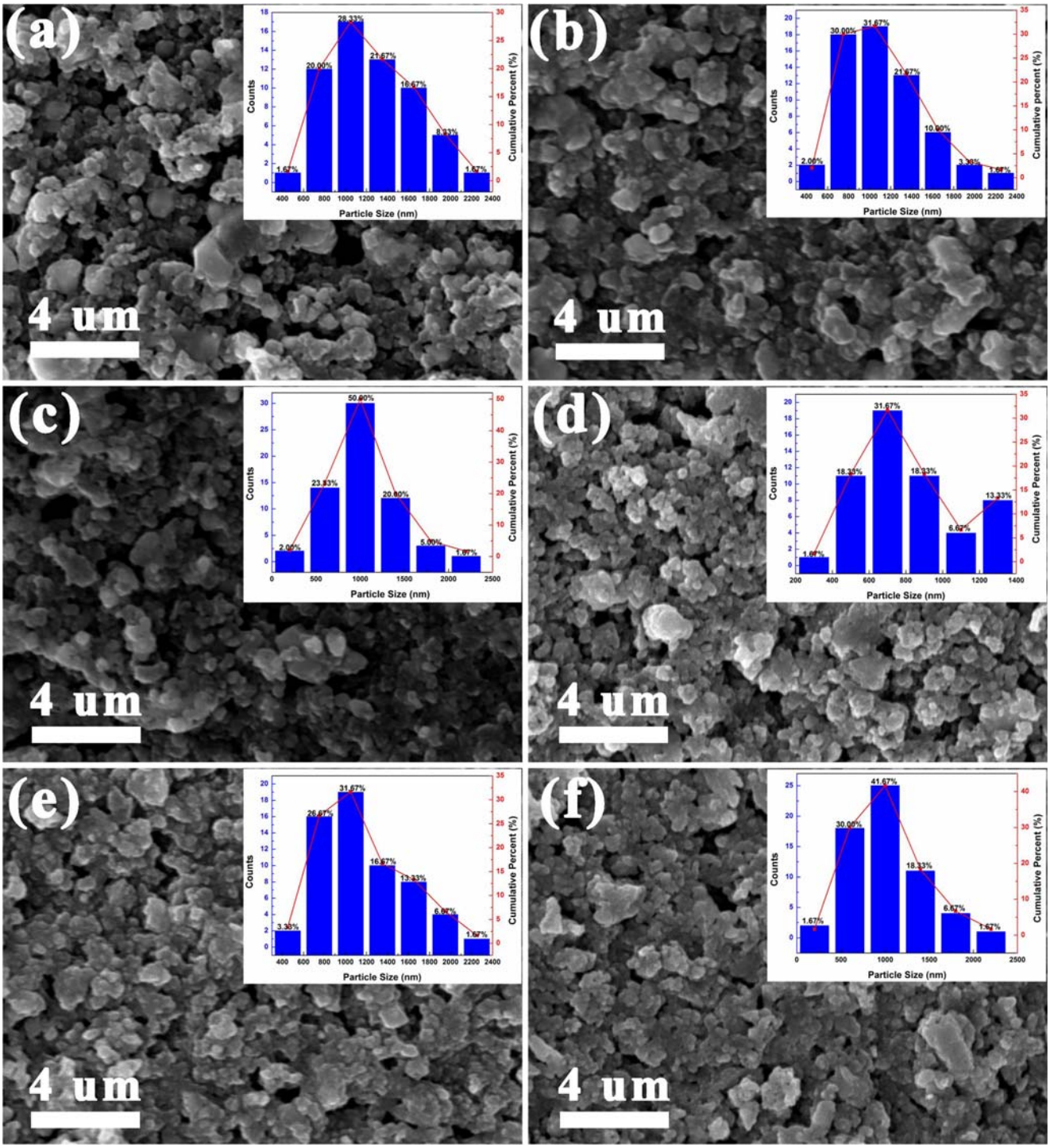

Fig. 5 SEM images of different adding amount: (**a**–**c**) $H_2Ti_3O_7$ and (**b**–**f**) TiO_2

capacity of 1% $H_2Ti_3O_7$ is 151.9 mAh g^{-1} at 0.5 C, while the 1% TiO_2 is 129.9 mAh g^{-1}. In other words, 1% of $H_2Ti_3O_7$ added provides better pathways for rapid ion diffusion. Besides, it is noted that with the increasing current rate, the discharge plateau shows a drop trend and the discharge capacity decreases for all samples.

Figure 6 d show the initial charge-discharge curves of 1% content $LiFePO_4/H_2Ti_3O_7$ and $LiFePO_4/TiO_2$ composite material at 0.5 C. Obviously, typically reversible voltages of ~3.4 V were displayed for $LiFePO_4/H_2Ti_3O_7$ and $LiFePO_4/TiO_2$, respectively, corresponding to the Fe^{3+}/Fe^{2+} redox couple. And the initial discharge capacities are 151.9 mAh g^{-1} and 129.9 mAh g^{-1} for two composites, which indicates that

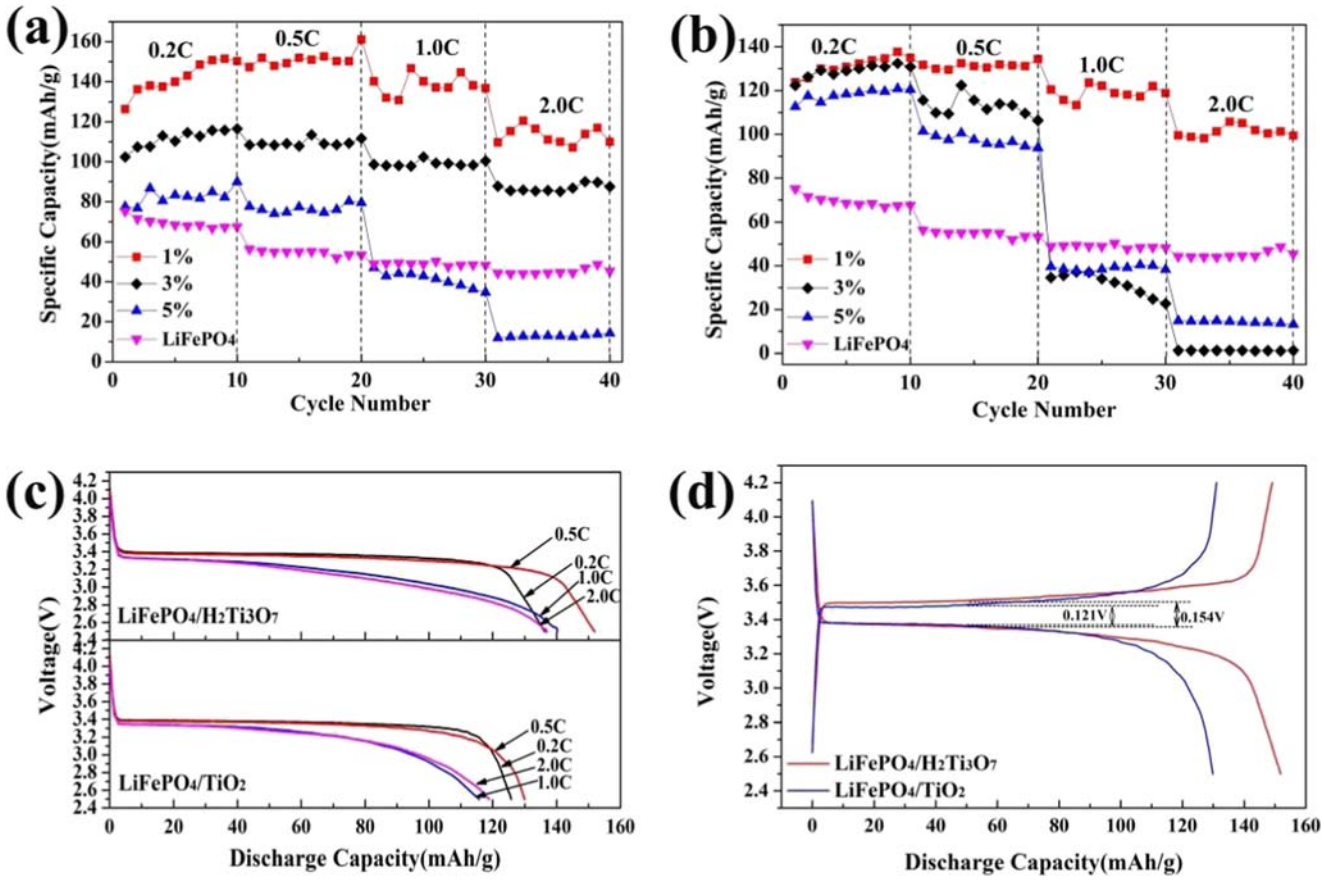

Fig. 6 **a**, **b** Rate capability of $LiFePO_4$ different amounts $LiFePO_4/H_2Ti_3O_7$ $LiFePO_4/TiO_2$ composite at different rate capability. **c** Discharge profiles of 1% $LiFePO_4/H_2Ti_3O_7$ and $LiFePO_4/TiO_2$ at various rates from 0.1 to 10 C. **d** Initial charge-discharge curves of 1% $LiFePO_4/H_2Ti_3O_7$ and $LiFePO_4/TiO_2$ composites

the electrochemical performance of $LiFePO_4$ is improved effectively after $H_2Ti_3O_7$ and TiO_2 were introduced. Additionally, the gap between charge and discharge plateaus for two samples is narrower, which demonstrating that the samples have lower overall resistance and can dramatically reduce the polarization.

Conclusions

In summary, the $LiFePO_4/H_2Ti_3O_7$ and $LiFePO_4/TiO_2$ samples were successfully synthesized via a simple sol-gel method. The introduction of $H_2Ti_3O_7$ and TiO_2 can reduce particle size and improve the uniformity of size distribution in a certain range. The $H_2Ti_3O_7$ and TiO_2 had a higher specific surface area than the $LiFePO_4$. The electrochemical performance of $LiFePO_4$ has been significantly improved after composited. Among all the samples, the 1% $H_2Ti_3O_7$ exhibited the best electrochemical properties with the maximum discharge capacity of 161.1 mAh g^{-1} and capacity retention is 105.83% at 0.5 C. Therefore, the appropriate introduction of $H_2Ti_3O_7$ is an efficient way to enhance the cycle stability and rate performance of $LiFePO_4$.

Funding information This work was financially supported by the National Natural Science Foundation of China (No.51674068, 51874079, 51771046, 51774002), Natural Science Foundation of Hebei Province (No.E2018501091), The Training Foundation for Scientific Research of Talents Project, Hebei Province (No.A2016005004), The Fundamental Research Funds for the Central Universities (No. N172302001, N182312007, N182306001), Hebei Province key research and development plan project (No.19211302D), and Qinhuangdao City University student of Science and Technology Innovation and Entrepreneurship Project (No. PZB1810008T-46, PZB1810008T-14).

References

1. Liu C, Luo S, Huang H, Zhai Y, Wang Z (2019) Low-cost layered $K_{0.45}Mn_{0.9}Mg_{0.1}O_2$ as a high-performance cathode material for K-ion batteries. ChemElectroChem. 6:2308–2315
2. Bao S, Luo S, Wang Z, Yan S, Wang Q (2019) Improving the electrochemical performance of layered cathode oxide for sodium-ion batteries by optimizing the titanium content. J Colloid Interface Sci 544:164–171

3. Li J, Luo S, Wang Q, Yan S, Feng J, Liu H, Ding X, He P (2018) Facile synthesis of carbon-$LiMnPO_4$ nanorods with hierarchical architecture as a cathode for high-performance Li-ion batteries. Electrochim Acta 289:415–421
4. Anh V, Qian Y, Andreas S (2012) Porous electrode materials for lithium-ion batteries-how to prepare them and what makes them special. Adv Energy Mater 2(9):1056–1085
5. Wang J, Hu Z, Yin X, Li Y, Huo H, Zhou J (2015) Alumina/phenolphthalein polyetherketone ceramic composite polypropylene separator film for lithium ion power batteries. Electrochim Acta 159:61–65
6. Scrosati, Bruno, Hassoun, Jusef, Sun Y (2011) Lithium-ion batteries. a look into the future. Energy Environ Sci 4(9):3287
7. Li J, Luo S, Sun Y, Li J, Zhang J, Yi T (2019) $Li_{0.95}Na_{0.05}MnPO_4$/C nanoparticles compounded with reduced graphene oxide sheets for superior lithium ion battery cathode performance. Ceram Int 45:4849–4856
8. Wu L, Lu J, Wei G, Wang P, Ding H, Zheng J, Li X, Zhong S (2014) Synthesis and electrochemical properties of $xLiMn_{0.9}Fe_{0.1}PO_4{\cdot}yLi_3V_2(PO_4)_3$/C composite cathode materials for lithium-ion batteries. Electhrochim Acta 146:288–294
9. Wu L, Zheng J, Wang L, Xiong X, Shao Y, Wang G, Wang J, Zhong S, Wu M (2019) PPy-encapsulated SnS_2 nanosheets stabilized by defects on a TiO_2 support as a durable anode material for lithium-ion batteries. Angew Chem Int Ed 58:811–815
10. Zhong S, Wu L, Liu J (2012) Sol-gel synthesis and electrochemical properties of $9LiFePO_4{\cdot}Li_3V_2(PO_4)_3$/C composite cathode material for lithium ion batteries. Electrochim Acta 74:8–15
11. Tao Y, Cao Y, Hu G, Chen P, Peng Z, Du K, Yong M, Xia H, Li L, Xie X (2019) Effects of vanadium oxide coating on the performance of $LiFePO_4$/C cathode for lithium-ion batteries. J Solid State Electrochem 23(7):2243–2250
12. Gong C, Xue Z, Wen S, Ye Y, Xie X (2016) Advanced carbon materials/olivine $LiFePO_4$ composites cathode for lithium ion batteries. Journal of Power Sources. 93-112
13. Eftekhari A (2017) $LiFePO_4$/C nanocomposites for lithium-ion batteries. J Power Sources:395–411
14. Zhang J, Luo S, Sui L, Sun Y, Niu Y (2018) Co-precipitation assisted hydrothermal method to synthesize $Li_{0.9}Na_{0.1}Mn_{0.9}Ni_{0.1}PO_4$/C nanocomposite as cathode for lithium ion battery. J Alloys Compd 768:991–994
15. Ma Z, Shao G, Wang X, Song J, Wang G (2013) $Li_3V_2(PO_4)_3$ modified $LiFePO_4$/C cathode materials with improved high-rate and low-temperature properties. J Ionics 19(12):1861–1866
16. Bao S, Luo S, Wang Z, Wang Q, Hao A, Zhang Y, Wang Y (2017) The critical role of sodium content on structure, morphology and electrochemical performance of layered P2-type $Na_xNi_{0.167}Co_{0.167}Mn_{0.67}O_2$ for sodium ion batteries. J. Power Sour 362:323–331
17. Medvedeva A, Pechen L, Makhonina E, Rumyantsev A, Koshtyal Y, Pervov V, Eremenko I (2019) Synthesis and electrochemical properties of lithium-ion battery cathode materials based on $LiFePO_4$-$LiMn_2O_4$ and $LiFePO_4$-$LiNi_{0.82}Co_{0.18}O_2$ composites. Russ J Inorg Chem 64(7):829–840
18. Liu J, Lin X, Han T, Li X, Gu C, Li J (2018) A novel litchi-like $LiFePO_4$ sphere/reduced graphene oxide composite Li-ion battery cathode with high capacity, good rate-performance and low-temperature property. Applied Surface Science. 233-241
19. Jun H, Myeongseong K, Yeon J, Lee G, Byung H, Lee S, Kwang C, Kwangbum K (2018) Rational design of oxide/carbon composites to achieve superior rate-capability via enhanced lithium-ion transport across carbon to oxide. J Mater Chem 6(14):6033–6044
20. Yang C, Hsu Y, Shih J, Wu Y, Chelladurail K, Tzong H, Lue S (2017) Preparation of 3D micro/mesoporous $LiFePO_4$ composite wrapping with porous graphene oxide for high-power lithium ion battery. Electrochem Acta 258:773–785
21. Li Y, Huang Y, Zheng Y, Huang R, Yao J (2019) Facile and efficient synthesis of α-Fe_2O_3 nanocrystals by glucose-assisted thermal decomposition method and its application in lithium ion batteries. J Power Sources 416:62–71
22. Huang Y, Li Y, Huang R, Yao J (2019) Ternary Fe_2O_3/Fe_3O_4/$FeCO_3$ composite as a high-performance anode material for lithium-ion batteries. J Phys Chem C 123:12614–12622
23. Zhang J, Luo S, Chang L, Hao A, Wang Z, Liu Y, Xu Q, Wang Q, Zhang Y (2017) Co-hydrothermal synthesis of $LiMn_{23/24}Mg_{1/24}PO_4{\cdot}LiAlO_2$/C nano-hybrid cathode material with enhanced electrochemical performance for lithium-ion batteries. Appl Surf Sci 394:190–196
24. Liu H, Luo S, Yan S, Wang Q, Hu D, Wang Y, Feng J, Yi T (2019) High-performance α-Fe_2O_3/C composite anodes for lithium-ion batteries synthesized by hydrothermal carbonization glucose method used pickled iron oxide red as raw material. Composites Part B 164:576–582
25. Bao S, Luo S, Wang Z, Yan S, Wang Q (2018) Novel high-capacity hybrid layered oxides $Na_xLi_{1.5-x}Ni_{0.167}Co_{0.167}Mn_{0.67}O_2$ as promising cathode materials for rechargeable sodium ion batteries. Ceram Int 44:22512–22519
26. Luo Y, Xu X, Zhang Y, Pi Y, Zhao Y, Tian X, An Q, Wei Q, Mai L (2014) Hierarchical carbon decorated $Li_3V_2(PO_4)_3$ as a bicontinuous cathode with high-rate capability and broad temperature adaptability. Adv Energy Mater 4(16)
27. Leng X, Wei S, Jiang Z, Lian J, Wang G, Jiang Q (2015) Carbon-encapsulated Co_3O_4 nanoparticles as anode materials with super lithium storage performance. Sci Rep 5(1):16629–16629